Coordinating Systematic Grid-Forming Control of Hybrid Photovoltaic Plants in Weak Grids

Shiwen Yu, *Graduate Student Member, IEEE*, and Lina He, *Senior Member, IEEE*

***Abstract*—With the anticipated integration of numerous hybrid photovoltaic (PV) plants into subtransmission and distribution grids, managing a mix of inverter-based energy resources such as PV systems and battery energy storage systems (BESS) becomes crucial. These resources are required to effectively coordinate for primary frequency (f) and voltage (V) control and participate in power sharing, particularly in weaker grids. Currently, inverter-based energy resources are predominantly coordinated by droop-based control, which proves inadequate for hybrid PV plants in more resistive subtransmission and distribution grids due to the tightly coupled active power (P) and reactive power (Q). To overcome this challenge, this paper proposes an innovative coordinating systematic primary control strategy for grid-forming inverters in hybrid PV plants based on the multiple-input and multiple-output (MIMO) decoupling control. This method adaptively decouples the connected subtransmission or distribution grids during operation, with the aim of achieving effective, coordinated, and independent primary f and V regulation and accurate power sharing. For verification, comparative case studies are conducted in Simulink between the proposed control strategy and a conventional droop control scheme. The findings indicate that our proposed control method facilitates autonomous and independent primary f and V control, along with precise power sharing without relying on communication links. This results in markedly enhanced steady-state and dynamic performance. The decentralized primary controller offers simplicity, robustness, and cost-effectiveness, contributing to the stability and resilience of utility grids.**

***Index Terms*—Coordinating systematic grid-forming control, hybrid PV plants, inverter-based energy resources, weak grids.**

I. Introduction

THE North American bulk power system is currently transitioning rapidly towards renewable energy sources to meet the national target of net zero emissions [1]. To promote the deployment of renewable energy, particularly PV sources, the concept of the hybrid PV plant has been proposed. These plants, typically exceeding 20 MW, are connected to medium-voltage subtransmission or distribution systems, operating between 34.5 kV and 115 kV [2], [3], [4], [5]. Hybrid PV plants are characterized by their diverse mix of inverter-based energy resources, including PV cells, wind turbines, and battery storage, all connected through a common outlet bus.

A significant challenge arises from the extensive integration of these inverter-based energy resources: the power grid experiences reduced inertia, making it susceptible to a large rate of change of frequency (ROCOF) and frequency oscillations during disturbances. Such conditions can activate under-frequency load-shedding relays, potentially causing cascading failures and power outages [6]. Consequently, maintaining grid reliability has become a major concern for power system operators. To mitigate these issues, it is essential for hybrid PV power plants to provide enhanced primary control services.

However, our team has found that existing primary control struggles with independent regulation for frequency and voltage within distribution grids due to the power coupling issue [7]. This situation highlights the need for considering the grid characteristics. This requirement gains further support from recent studies that examine the impact of grid impedance on inverter-based energy resources via small-signal stability and sensitivity analysis [8], [9]. To solve this challenge, all the sources in a hybrid PV power plant need to operate collaboratively in a way that is internally coordinated.

Primary control coordination of inverter-based energy resources within a hybrid PV plant traditionally relies on communication-based strategies, including centralized control [10], [11], master-slave control [12], and distributed control [13]. These methods use global or local communication networks to set current references for averaged power sharing. However, the communication infrastructure introduces vulnerabilities, such as susceptibility to time latency, cyber-attacks, and stability problems. Additionally, these inverter-based energy resources typically use existing commercial grid-following (GFL) inverters that operate as current sources. They regulate P and Q output by merely tracking the grid voltage and angle using phase-locked loops (PLLs). As the penetration level increases, these methods are unable to actively regulate f and V to support the grid, which significantly reduces the system inertia. Furthermore, the PLL can lead to stability issues in phase or voltage disturbances caused by noise and load transients.

In contrast, existing GFM controls, such as droop control [14], [15], virtual synchronous generator [16], [17], and virtual oscillator control [18], enable inverter-based energy resources to actively control f and V. These controls facilitate internal coordination without relying on communication links. Despite these advantages, they pose significant challenges to power system

Manuscript received 13 February 2024; accepted 16 March 2024. Date of publication 2 April 2024; date of current version 1 May 2024. *(Corresponding author: Lina He.)*

The authors are with the Department of Electrical and Computer Engineering, University of Illinois Chicago, Chicago, IL 60607 USA (e-mail: syu@uic.edu; lhe@uic.edu).

Digital Object Identifier 10.1109/TICPS.2024.3384332

2832-7004 © 2024 IEEE. Personal use is permitted, but republication/redistribution requires IEEE permission.
See https://www.ieee.org/publications/rights/index.html for more information.

Authorized licensed use limited to: ULAKBIM UASL - Omer Halisdemir Universitesi. Downloaded on November 17,2024 at 06:12:21 UTC from IEEE Xplore. Restrictions apply.

stability. They were originally developed for highly inductive transmission systems based on the active power-frequency (P-f) and reactive power-voltage (Q-V) droop mechanisms [19]. However, in subtransmission and distribution power systems where P and Q are highly coupled due to resistive network characteristics, these control strategies fail to provide independent and effective primary control and result in inaccurate power sharing [20]. Additionally, GFM controls are primarily optimized for standalone operation, which can compromise the desired dynamic and stability performance when connected to the grid [21], [22].

Several variants of GFM methods have been proposed to overcome the challenge of power coupling in resistive networks, including virtual impedance control and virtual frame transformation control [23], [24]. Virtual impedance control works by increasing the output impedance of inverters via an additional virtual inductor in the voltage control loop. However, this approach can inadvertently amplify voltage harmonics and destabilize voltage control during transient events [23]. On the other hand, virtual frame transformation control approaches the coupling issue as a matter of orthogonal frame transformation [24]. In this method, f and V are transformed into a virtual frame that eliminates the coupling relationship between them.

However, these methodologies focus on addressing the coupling issue within the inverter system, particularly caused by the output impedance of filters and connection lines. The underlying reason for this focus is that these schemes simplify the power grid as an ideal Thevenin equivalent circuit, thereby overlooking the intrinsic coupling challenges present in power grids. Such an oversimplification disregards the complex, inherent nature of the grid and does not account for its time-varying characteristics, which are influenced by disturbances, faults, and load variations. This assumption limits their effectiveness when connected to the actual power grid, as they fail to provide efficient, coordinated, and independent primary control for inverter-based energy resources. Moreover, the significant influence of large power plants on the overall power balance and V and f regulation within the weak grid is a critical aspect that remains unexplored in existing studies. Therefore, a comprehensive analysis of these impacts and the development of an appropriate strategy are essential steps in addressing these complex grid integration challenges.

To solve these challenges, this paper presents an innovative coordinating systematic primary control approach for GFM inverters in hybrid PV plants, tailored to address the coupling issues present in power grids. It employs the time-varying impedance concept from [25], which has been shown to effectively identify online voltage instability within bulk power systems with high voltage direct current (HVDC) integrated with offshore wind energy. Furthermore, the proposed control strategy is a GFM primary control, which is inherently communication-free and autonomously operates on local measurements and actions. It is applicable for all resources, thus significantly waiving communication costs and avoiding cyber-attacks. The effectiveness of this control strategy is rigorously evaluated in terms of independent f and V regulation, stability enhancement, and power-sharing capabilities. The case study employs a detailed power grid model, which consists of subtransmission and distribution subgrids adapted from the IEEE 14 bus system, to conduct simulations in MATLAB/Simulink. Compared with the traditional GFM control, the proposed control significantly improves the power-sharing capability in steady state and dynamic performance during disturbances such as reference steps, three-phase short circuit faults, and load variations.

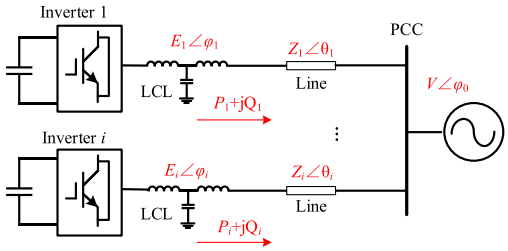

Fig. 1. Parallel connected inverter-based energy resources.

This paper is organized as follows. Section II introduces the design of the coordinating GFM control. In Section III, the small-signal stability analysis for the proposed controller is conducted. Section IV shows the simulation results of the case study and an in-depth analysis. Section V concludes the paper.

II. Coordinating Systematic Primary Control Design

This section details the design of the proposed primary control for inverter-based energy resources, tailored to the coupling characteristics of subtransmission/distribution grids.

A. Conventional Droop-Based GFM Control

Fig. 1 shows a single-line model of inverter-based energy resources connected in parallel within a power grid, which is widely used in existing studies. Each inverter-based energy resource interfaces with an LCL filter and connects to the grid via a line. The main power grid is usually simplified as an ideal voltage source behind the point of common coupling (PCC).

The power flow of P and Q from the i_{th} source can be expressed as the function of its output terminal voltage, the voltage at the outlet bus, and the impedance between them:

$$P_i = \frac{E_i V}{Z_i}\sin\delta_i \sin\theta_i + \frac{{E_i}^2 - E_i V\cos\delta_i}{Z_i}\cos\theta_i \tag{1}$$

$$Q_i = -\frac{E_i V}{Z_i}\sin\delta_i \cos\theta_i + \frac{{E_i}^2 - E_i V\cos\delta_i}{Z_i}\sin\theta_i \tag{2}$$

where P_i and Q_i are the output active and reactive power of the i_{th} inverter, respectively; $E_i\angle\varphi_i$ is the terminal voltage of the i_{th} inverter; $V\angle\varphi_0$ is the nominal voltage of the power system; δ_i is the power angle difference between the i_{th} inverter and the grid voltage, which is given by $\varphi_i - \varphi_0$; $Z_i\angle\theta_i$ represents the impedance of the filter and the connection line; θ_i is the impedance angle. The whole system is a multiple-input and multiple-output (MIMO) system with input of φ_i and E_i, and output of P_i and Q_i, respectively, as depicted in Fig. 2.

In Fig. 2, there is coupling between the output active and reactive power due to the existence of complex impedance, i.e.,

Authorized licensed use limited to: ULAKBIM UASL - Omer Halisdemir Universitesi. Downloaded on November 17,2024 at 06:12:21 UTC from IEEE Xplore. Restrictions apply.

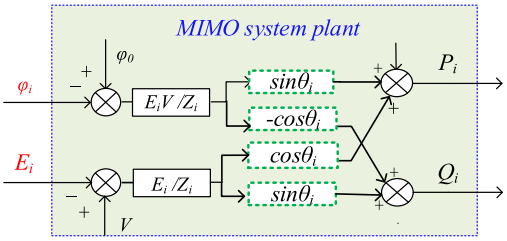

Fig. 2. Block diagram of a MIMO system.

$Z_i\angle\theta_i$. This coupling will degrade the dynamic and stability performance of the control system, leading to considerable overshoot and oscillation.

In a traditional transmission system, the line impedance is inductance-dominated ($\theta_i \approx 90°$), And the phase angle difference is small ($\delta_i \approx 0°$). Therefore, (1) and (2) can be simplified as (3) and (4), respectively [14], [15].

$$P_i = \frac{E_i V}{Z_i}\,\delta_i \tag{3}$$

$$Q_i = \frac{E_i^2 - E_i V}{Z_i} \tag{4}$$

This enables the droop-based GFM inverter control to be applicable in transmission systems, as shown in (5)–(6).

$$f_i - f^0 = m\left(P_i^{set} - P_i\right) \tag{5}$$

$$E_i - E^0 = n\left(Q_i^{set} - Q_i\right) \tag{6}$$

where f_i and E_i are references of output frequency and voltage for the i_{th} ($i = 1, 2, \ldots k$) inverter; f^0 and E^0 are the uniform nominal values of frequency and voltage for all inverters in a hybrid power plant; P_i^{set} and Q_i^{set} are setpoints of P and Q of the i_{th} inverter, which are determined by power dispatch; P_i and Q_i are the actual output P and Q; the $(P_i^{\min},\ P_i^{\max})$ and the $(-Q_i^{\max},\ Q_i^{\max})$ are the operational ranges for P and Q, respectively. m and n are the per-unit positive coefficients for P-f droop and Q-V droop.

To ensure average power sharing, all inverters use the same m and n in P-f and Q-V droop control. This can ensure that when f and V change (Δf and ΔV) due to load variations, changes in output power (ΔP_i, and ΔQ_i) will be adjusted autonomously and be proportional to their power ratings, i.e., P_i^r, and Q_i^r, as shown in (7) and (8). It is noted that values of f, V, P, and Q are actual measurements to show the power-sharing mechanism among the inverters.

$$m = \frac{\Delta f}{f^0}\Big/\frac{\Delta P_1}{P_1^r} = \frac{\Delta f}{f^0}\Big/\frac{\Delta P_2}{P_2^r} = \cdots = \frac{\Delta f}{f^0}\Big/\frac{\Delta P_k}{P_k^r} \tag{7}$$

$$n = \frac{\Delta E}{E^0}\Big/\frac{\Delta Q_1}{Q_1^r} = \frac{\Delta E}{E^0}\Big/\frac{\Delta Q_2}{Q_2^r} = \cdots = \frac{\Delta E}{E^0}\Big/\frac{\Delta Q_k}{Q_k^r} \tag{8}$$

However, as indicated in [7], traditional droop control faces issues in hybrid PV plants within medium voltage subtransmission/distribution networks due to their complex impedance. This complexity invalidates the assumption of purely inductive impedance, undermining the independent regulation of f and V and hampering accurate power sharing. In extreme situations, it can result in system instability, severe device damage, or even widespread outages. Thus, it is crucial to consider the characteristics of the main grid in control design.

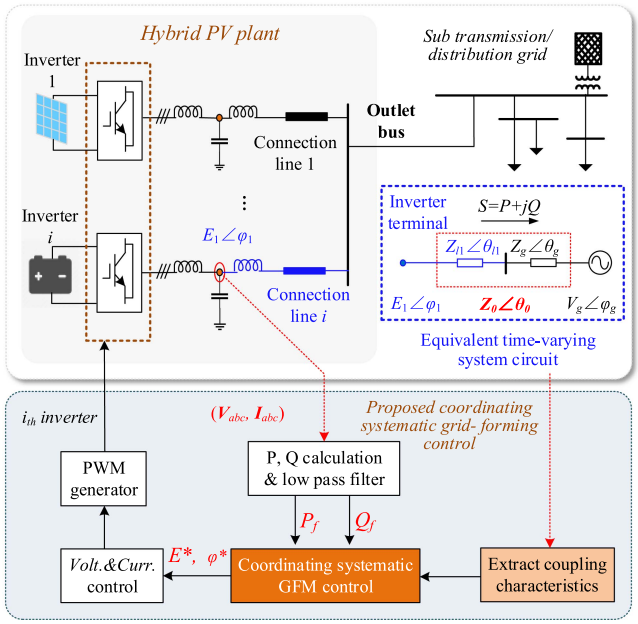

Fig. 3. Overall scheme for the proposed coordinating systematic GFM control for inverter-based energy resources in hybrid PV plant.

B. Proposed Coordinating Systematic GFM Control

To overcome the challenges mentioned above, the proposed coordinating systematic GFM control is proposed based on the principle of decoupling the power grid. It can enable inverters to independently control f and V and accurately share power, thus achieving efficient coordination among the inverter-based energy resources. Fig. 3 shows the overall control configuration in parallel-connected inverter-based energy resources within a hybrid power plant.

In Fig. 3, the inverter-based energy resources are interconnected via a shared outlet bus linked to the subtransmission/distribution grid. The node between the two inductors of the LCL filter is considered the inverter terminal. Its voltage and current are measured and sent to the control system as input signals. The control system is unified for all the inverters in a hybrid power plant. This control system, standardized for all inverter-based energy resources in the plant, aims to achieve optimal coordination by decoupling not just the inverter system but also the external grid elements, including the power grid, filters, and connection lines.

In the proposed GFM control strategy, the coupling characteristics of the external system are continuously extracted and fed into the control system to update its parameters. This dynamic approach enables the adaptive decoupling of P and Q, allowing the controller to respond effectively to varying grid conditions in the subtransmission/distribution grid. To accurately extract these coupling characteristics, we model the external system from the

Authorized licensed use limited to: ULAKBIM UASL - Omer Halisdemir Universitesi. Downloaded on November 17,2024 at 06:12:21 UTC from IEEE Xplore. Restrictions apply.

perspective of the inverter terminal using an equivalent circuit. The circuit consists of time-varying components: a time-varying impedance $Z_0\angle\theta_0$ and a time-varying voltage source $V_g\angle\varphi_2$, which can reflect the dynamics of the power grid during online operation. The parameters are updated in real time. Specifically, $Z_0\angle\theta_0$ represents the combined impedance of the outside system, consisting of the filter, connection line, and power grid, as seen in Fig. 3 and (9).

$$Z_0\angle\,\theta_0 = Z_{l1}\,\angle\theta_{l1} + Z_g\angle\theta_g \tag{9}$$

Where $Z_{l1}\angle\theta_{l1}$ denotes the impedances of the first two parts, which are constant and can be easily known from plant and grid operators. The impedance of the power grid is time-varying and can be determined online based on real-time voltage and current measurements at the outlet bus during events, as shown in (10).

$$Z_g\angle\,\theta_g = \frac{\vec{V}_1 - \vec{V}_2}{\vec{I}_1 - \vec{I}_2} \tag{10}$$

where $\vec{V}_1$and $\vec{I}_1$ represent the voltage and current phasors measured at the first sampling time, while $\vec{V}_2$ and $\vec{I}_2$ represent the measurements at the second sampling time, respectively. The grid impedance voltage, i.e., $V_g\angle\varphi_g$, can be calculated as indicated in (11).

$$V_g\angle\,\varphi_g = \vec{V}_2\ - Z_g\angle\theta_g * \vec{I}_2 \tag{11}$$

By substituting the time-varying impedance $Z_0\angle\theta_0$ in (1) and (2) and considering the approximations including $\sin\varphi \approx \varphi$ and $\cos\varphi \approx 1$, (12) is derived.

$$\begin{bmatrix} P_i \\ Q_i \end{bmatrix} = \begin{bmatrix} \sin\theta_0 & \cos\theta_0 \\ -\cos\theta_0 & \sin\theta_0 \end{bmatrix} \begin{bmatrix} \frac{E_i V_g \varphi_0}{Z_o} \\ \frac{E_i(E_i - V_g)}{Z_o} \end{bmatrix} \tag{12}$$

It can be seen that the P_i and Q_i are coupled with φ_0 and E_i, which can be decoupled by a time-varying decoupling matrix $\boldsymbol{D} = \begin{bmatrix} \sin\theta_0 & -\cos\theta_0 \\ \cos\theta_0 & \sin\theta_0 \end{bmatrix}$, as shown in (13).

$$\begin{bmatrix} P_d \\ Q_d \end{bmatrix} = \begin{bmatrix} \sin\theta_0 & -\cos\theta_0 \\ \cos\theta_0 & \sin\theta_0 \end{bmatrix} \begin{bmatrix} P_i \\ Q_i \end{bmatrix} = \begin{bmatrix} \frac{E_i V_g \varphi_0}{Z_o} \\ \frac{E_i(E_i - V_g)}{Z_o} \end{bmatrix} \tag{13}$$

By applying the time-varying impedance-based decoupling matrix, the P_i and Q_i are transformed into decoupled forms P_d and Q_d, respectively. These decoupled powers now have a linear relationship with the φ_0 and E_i, as depicted in (3) and (4). This decoupling makes droop control a viable option for coordinating the inverter. Based on this insight, the proposed coordinating systematic GFM control is shown in Fig. 4.

Its core innovation is the coordinating systematic GFM controller, which integrates a decoupling matrix with droop control principles, as detailed in (14) and (15).

$$f - f_0 = m_i\ [(P_{set} - P_f)\sin\theta_0 - (Q_{set} - Q_f)\cos\theta_0)] \tag{14}$$

$$E - E_0 = n_i\ [(P_{set} - P_f)\cos\theta_0 + (Q_{set} - Q_f)\sin\theta_0)] \tag{15}$$

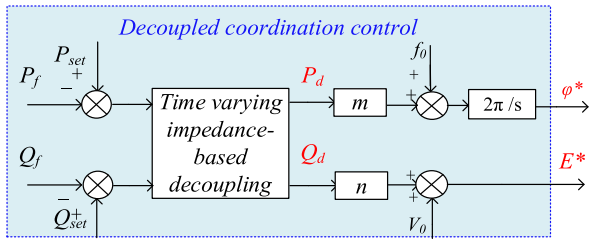

Fig. 4. Proposed coordinating systematic GFM control.

In Fig. 4, the inputs of the proposed coordinating systematic GFM controller are the filtered power measurements, i.e., P_f and Q_f. m and n are droop coefficients; f_0 and V_0 are the nominal values of frequency and voltage magnitude, respectively; E^* is the magnitude reference and φ^* is the phase reference for the output voltage, which will be sent to the pulse width modulation (PMW) generator, which modulates the inverter switches. This configuration ensures two primary benefits: (1) independent regulation of output f and V by eliminating the coupling between P and Q, which increases the system stability, and (2) rapid, efficient, and accurate power sharing among inverters.

III. Small-Signal Stability Analysis and Parameter Design

This section delves into the stability analysis and parameter design of the proposed coordinating systematic GFM controller by deriving a small-signal model for a hybrid PV plant.

A. Small-Signal Stability Analysis

The small-signal stability analysis begins by linearizing the dynamics of P and Q for each inverter, as shown in (12). This process results in (16) and (17), which detail the small-signal dynamics.

$$\Delta P = \frac{1}{Z_0}\ [(EV_g\Delta\varphi + \Delta EV_g\varphi)\sin\theta_0 + \Delta E\,(2E - V_g)\cos\theta_0] \tag{16}$$

$$\Delta Q = \frac{1}{Z_0}\ [-(EV_g\Delta\varphi + \Delta EV_g\varphi)\cos\theta_0 + \Delta E\,(2E - V_g)\sin\theta_0] \tag{17}$$

where the symbol Δ is used to represent small-signal variations. Based on (13), the small-signal values of decoupled P and Q can be expressed as follows:

$$\Delta\,P_d = \Delta P\sin\theta - \Delta Q\cos\theta\ = \frac{1}{Z_0}\ (EV_g\Delta\varphi + \Delta EV_g\varphi) \tag{18}$$

$$\Delta\,Q_d = \Delta P\cos\theta + \Delta Q\ \sin\theta = \frac{1}{Z_0}\ \Delta E\,(2E - V_g) \tag{19}$$

Authorized licensed use limited to: ULAKBIM UASL - Omer Halisdemir Universitesi. Downloaded on November 17,2024 at 06:12:21 UTC from IEEE Xplore. Restrictions apply.

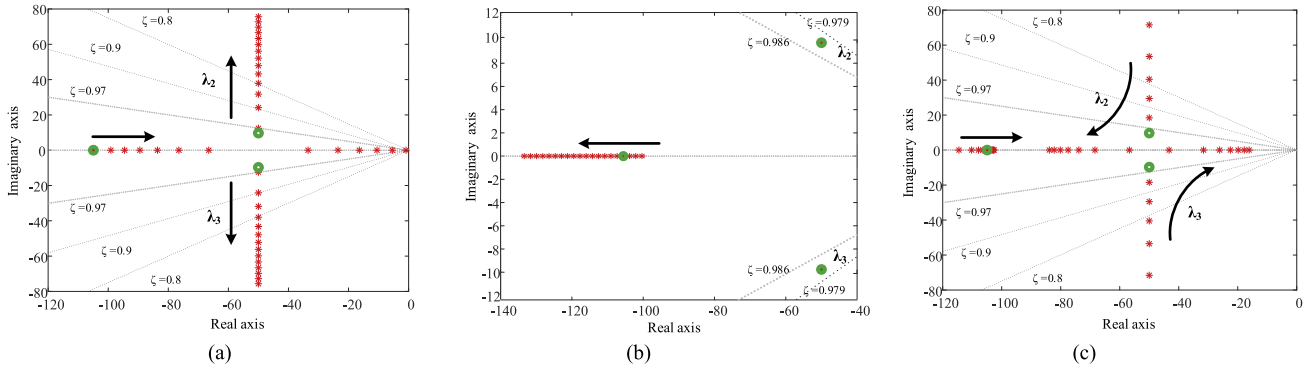

Fig. 5. Root locus diagrams. (a) Increase *m* with fixed *n*, (b) increase *n* with fixed *m*, and (c) increase SCR with fixed *m* and *n*.

In the proposed coordinating systematic GFM controller for inverters, the dynamics of power measurements from the low-pass filter are modeled using a first-order inertial element. This model is integrated into the droop control mechanism. By replacing $\Delta\varphi$ with $2\pi\Delta f/\mathrm{s}$, the small-signal model can be represented as (20) and (21).

$$\Delta f = -\frac{m}{Z_0\left(1+T_f s\right)}\left(EV_g\frac{2\pi\Delta f}{s}+\Delta EV_g\varphi\right) \tag{20}$$

$$\Delta E = -\frac{nV_g\varphi}{Z_0\left(1+T_f s\right)} \tag{21}$$

where T_f is the sampling time of the filters, which can be calculated from $1/w_f$; w_f denotes the cut-off frequency of the low pass filters. It's noted that the dynamics of the inner loop voltage and current controls are relatively fast and are ignored. By combining (20) and (21), the resulting characteristic equation of the system is of the third order, as shown (22).

$$s^3\Delta\hat{f}+As^2\Delta\hat{f}+Bs\Delta\hat{f}+C\Delta\hat{f}=0 \tag{22}$$

where

$$A = \frac{2Z_0+n\left(2E-V_g\right)}{Z_0T_f}$$

$$B = \frac{2\pi T_f mEV_g+n\left(2E-V_g\right)+Z_0}{Z_0{T_f}^2}$$

$$C = \frac{2\pi Z_0 mEV_g+2\pi mnEV_g\left(2E-V_g\right)}{{Z_0}^2T_f^2}$$

B. Parameter Design Considering System Stability

This section focuses on designing parameters for the proposed controller. Based on (21), the eigenvalue analysis is conducted to explore how variations in these parameters affect the small-signal stability of the system. Specifically, critical parameters $\sin\theta$ and $\cos\theta$ are set based on the system impedance during online operation to ensure efficient decoupling of P and Q. The droop coefficients are related to the power-sharing capability of the inverter. An increase in these coefficients generally enhances power sharing. To evaluate the corresponding control stability, the droop coefficients are changed to plot the root locus diagrams.

Fig. 5(a) shows the trace of eigenvalues as the P-f droop parameter m is increased. The arrows show the evolution direction of the eigenvalues. As m increases, the eigenvalues $\lambda_{2,\,3}$ diverge from the zero axis, resulting in a reduced damping factor (ζ). This indicates that there is a tradeoff between enhancing power-sharing capabilities in the inverter and the overall system damping. Fig. 5(b) shows the behavior of eigenvalues with increasing droop coefficient n. It shows that there is no significant shift in $\lambda_{2,\,3}$ and thus no impact on damping. In both cases, the eigenvalues remain in the left half-plane, which indicates that stable power sharing among inverters can be achieved via careful adjustment of m and n.

To achieve maximum power-sharing among inverters, the actual values of the m and n for each inverter, i.e., m_{act} and n_{act} are determined based on the maximum allowed frequency and voltage variations, i.e., $\Delta f_{\max}$ and $\Delta E_{\max}$ according to the grid code, respectively. Additionally, the maximum decoupled P and Q values of each inverter are also factored into this calculation, as expressed in (23) and (24).

$$m_{act} = \frac{\Delta f_{\max}}{|P_d|_{\max}} \tag{23}$$

$$n_{act} = \frac{\Delta E_{\max}}{|Q_d|_{\max}} \tag{24}$$

where

$$P_d = P_{rating}\ \sin\theta - Q_{rating}\cos\theta$$

$$Q_d = P_{rating}\ \cos\theta + Q_{rating}\sin\theta$$

In Fig. 5(a) and (b), the eigenvalues associated with the optimized droop coefficients m and n (m_{act} and n_{act}) are marked in green. These eigenvalues confirm that the selected m_{act} and n_{act} values ensure robust damping and stable operation of the system. Fig. 5(c) shows the root locus diagram of the system to analyze the controller robustness under different grid impedance conditions. This diagram reveals that regardless of the system impedance variations, the poles stay in the left half-plane, indicating that the proposed controller can work stable in a wide range of systems/conditions.

Authorized licensed use limited to: ULAKBIM UASL - Omer Halisdemir Universitesi. Downloaded on November 17,2024 at 06:12:21 UTC from IEEE Xplore. Restrictions apply.

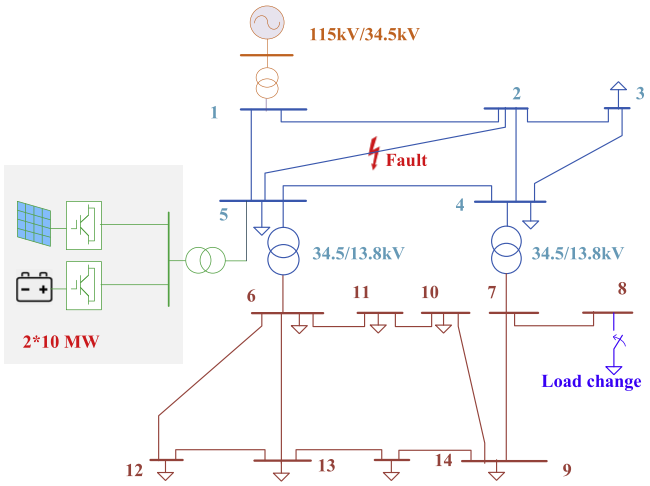

Fig. 6. Benchmark system based on IEEE 14 bus system.

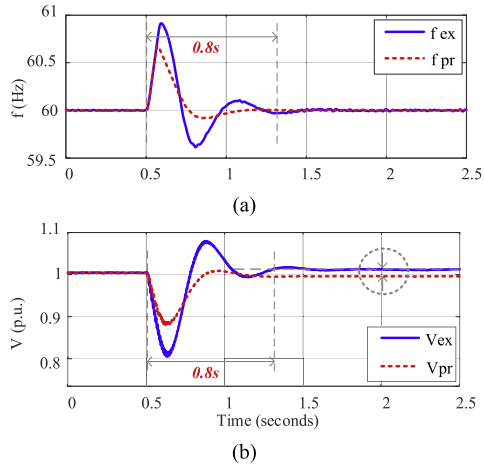

Fig. 7. Simulation of a f step response. (a) F performance and (b) v performance.

IV. Simulation Results

The performance of the proposed control strategy is rigorously tested via comprehensive simulation case studies conducted in MATLAB/Simulink. Our simulation framework replicates an electrical power grid composed of two key components: a 34.5 kV subtransmission grid and a 13.8 kV distribution grid. These grids are interconnected with a 115 kV bulk power system, which is modeled using a swing bus. The power grid is depicted in Fig. 6.

The network and load details of our system are derived from the IEEE 14-bus system, as referenced in [26]. The hybrid PV plant is integrated into the grid at bus 5 via a 34.5 kV/480 V transformer. This plant consists of two inverter-based energy resources: a PV system and a BESS, with identical capacity of 10 MW each. The parameters are shown in Table I. This case study conducts a comparative analysis of two GFM control strategies: our newly developed coordinating systematic GFM control (termed "proposed control" henceforth) and the conventional droop-based GFM control (referred to as "existing control"). The evaluation rigorously examines their performance across four scenarios: (1) V step response, (2) f step response, (3) a three-phase short circuit fault in the power grid, and (4) variations in load within the power system. utilizing MATLAB/Simulink for simulations.

The simulation data, particularly the f, V, P, and Q trajectories for both control strategies are depicted in this section. The trajectories for the existing control are labeled as (f_{ex}, V_{ex}, P_{ex}, Q_{ex}) and for the proposed control as (f_{pr}, V_{pr}, P_{pr}, Q_{pr}). It should be noted that these trajectories, reflecting the outputs of both inverter-based energy resources at bus 5, underscore the coordination capability of the proposed control.

A. Case I: Frequency Step Response

This case compares the f step response of the inverter-based energy resources using the existing control with the proposed control under an identical condition, specifically a 2.5% f step change at 0.5 s. Their simulation results are shown in Fig. 7.

In Fig. 7(a), the f response (f_{ex}) under the existing control demonstrates significant fluctuations with pronounced peaks and valleys, requiring 0.8 s to settle. The lowest frequency reached is close to the typical UFLS threshold of 59.5 Hz. This proximity, coupled with the extended stabilization time, raises concerns about potential UFLS relay activation during more intense disturbances [27]. Fig. 7(b) examines the V response (V_{ex}) behavior of the inverter using the existing control. Here, we observe a considerable voltage drop, about 20%, followed by an underdamped oscillatory pattern taking the same 0.8 s to stabilize. Furthermore, the V does not revert to its nominal value in the steady state following the fluctuation. This finding indicates a strong impact of the f disturbance on V, suggesting a coupling between V and f controls.

In Fig. 7(a), the f trajectory (f_{pr}) of the inverter using the proposed control shows a modest dip of 12% and quickly returns to nominal, with an improved settling time due to the influence of the larger-scale transmission system. The frequency nadir improves by 0.3 Hz, reducing the risk of triggering UFLS. In Fig. 7(b), the V trajectory (V_{pr}) under the proposed control also recovers swiftly to nominal within 0.5s, demonstrating superior V regulation compared to the existing control, which exhibits more pronounced oscillations in response to disturbances in f and V. Overall, the proposed control exhibits a better-damped response compared to the existing control. In addition, it enables the inverter-based energy resources to maintain independent and coordinated V control, even when faced with f disturbances.

B. Case II: Voltage Step Response

This part of the study examines how the V step response differs between the proposed control and the existing control strategy. The test condition involves a 5% step change in the V reference occurring at 0.5 s. Fig. 8 illustrates the resulting f and V performance under both control methodologies.

Fig. 8(a) demonstrates that the proposed control leads to a significant enhancement in the dynamic and stability performance of the IBRs. When subjected to a V step change, the V trajectory

Authorized licensed use limited to: ULAKBIM UASL - Omer Halisdemir Universitesi. Downloaded on November 17,2024 at 06:12:21 UTC from IEEE Xplore. Restrictions apply.

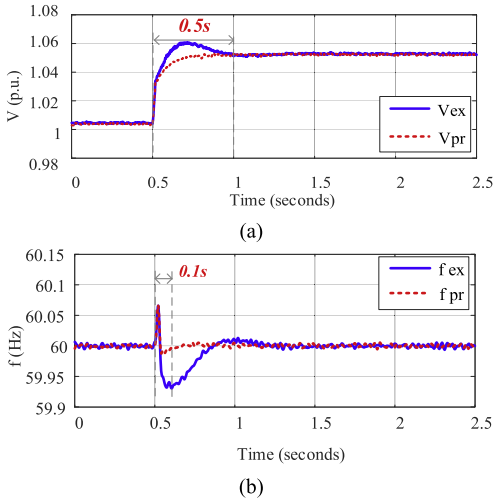

Fig. 8. Simulation of a V step response. (a) V performance and (b) f performance.

under the existing control (V_{ex}) temporarily overshoots to 1.05 p.u.. However, this adjustment causes noticeable instability in the f trajectory (f_{ex}), which takes around 0.5 s to settle. This response underscores the vulnerability of the IBRs to voltage step changes under the existing control framework. In contrast, the proposed control results in a more controlled increase in the V trajectory (V_{pr}) to 1.05 p.u., effectively mirroring the 5% step change in the V reference. Moreover, the f trajectory under the proposed control (f_{pr}) shows only mild fluctuations and quickly returns to its nominal value within less than 0.1 s.

These outcomes demonstrate a marked improvement in the dynamic performance of the inverters with the proposed control. The proposed method facilitates an independent and more effectively damped regulation of both f and V. This independence is crucial for enhancing the overall stability and responsiveness of the inverter-based energy resources.

C. Case III: Three-Phase Short Circuit Fault

This case study aims to assess the transient stability of the inverters in the event of a three-phase short circuit fault occurring near bus 5 in the power grid. The fault is introduced at 0.5 s and persists for 0.1 s. Fig. 9 compares the f and V performance of both control schemes during this event.

Fig. 9(a) shows that under the existing control, the V trajectory (V_{ex}) drops to 0.6 p.u. immediately upon fault occurrence and remains low for one cycle, then spikes to 1.4 p.u. and falls to 0.5 p.u. at 0.8 s post-fault. The f trajectory (f_{ex}) oscillates significantly from the fault onset but returns to nominal, with noticeable fluctuations. This behavior is attributed to the inability of the existing control to provide sufficient damping to counteract the post-fault instability. With the proposed control shown in Fig. 9(b), the V trajectory (V_{pr}) decreases to 0.6 p.u. during the fault but exhibits improved support, recovering to nominal with minimal oscillation. The f trajectory (f_{pr}) also shows reduced oscillation, momentarily dipping below 59.5 Hz for about 0.05 s, significantly less than the minimum delay threshold of six cycles

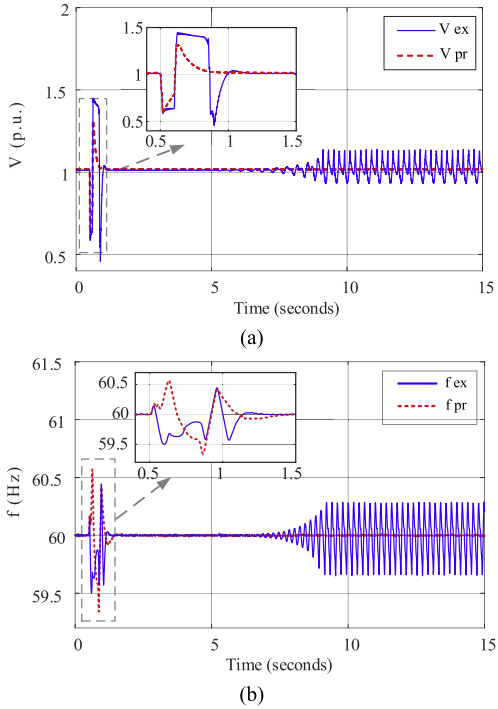

Fig. 9. Simulation of a three-phase short circuit fault. (a) V performance and (b) f performance.

(0.1 s) required by the SERC UFLS Standard. This ensures that the load is not disconnected prematurely, allowing the f to return to its normal range [27]. The results thus confirm that the proposed control strategy enables the inverters to offer well-damped f and V regulation during recovery from fault events, thereby stabilizing the system against post-fault instability.

D. Case IV: Simulation of Load Variation

This case study aims to evaluate the effectiveness of the proposed control in managing coordinated power sharing among inverters. For this purpose, a 10 MW load with a power factor of 0.9 is introduced to bus 8 in the power grid at 0.5 s. Fig. 10 displays the responses in f, V, P, and Q of the inverters.

As shown in Fig. 10(a) and (b), The application of droop control results in an unsatisfactory dynamic performance of the inverter-based energy resources as observed in their V and f trajectories. The V trajectory (V_{ex}) experiences a dip of 0.08 p.u. and takes about 0.1 s to stabilize at 0.98 p.u. following severe fluctuation. The f trajectory (f_{ex}) displays a notable drop of 0.2 Hz and requires 0.25 s to return to its nominal value. Furthermore, as shown in Fig. 10(c) and (d), the load step results in severe oscillations in both the P and Q trajectories (P_{ex} and Q_{ex}), which highlights the coupling issue in the subtransmission/distribution grid. This issue hinders the coordination capabilities of the inverter-based energy resources, resulting in decreased system stability and reliability.

Conversely, the proposed control mechanism significantly improves inverter performance during load variations, with the V trajectory (V_{pr}) quickly recovering to its pre-event value within

Authorized licensed use limited to: ULAKBIM UASL - Omer Halisdemir Universitesi. Downloaded on November 17,2024 at 06:12:21 UTC from IEEE Xplore. Restrictions apply.

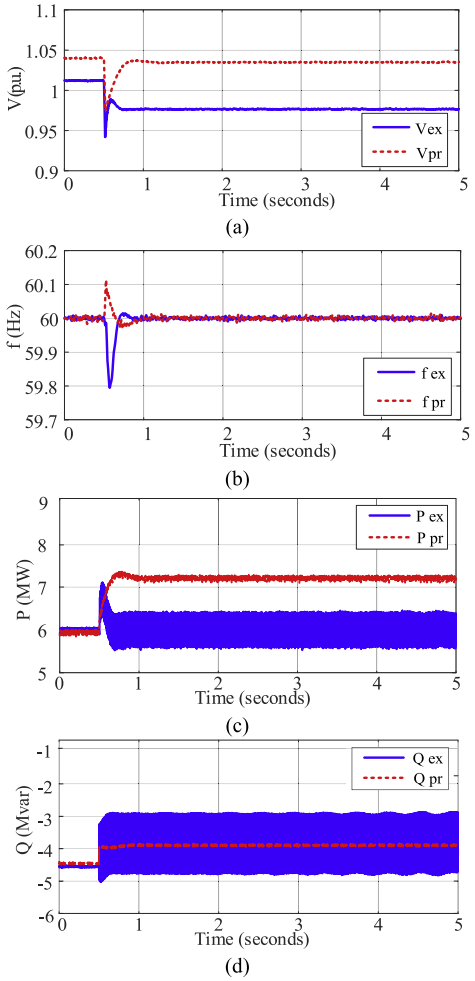

Fig. 10. Simulation of a load variation. (a) V performance, (b) f performance, (c) output P of inverters, and (d) output Q of inverters.

0.3 s after a minor dip of 0.07 p.u., and the f trajectory (f_{pr}) stabilizing at nominal within 0.25 s after a slight 0.1 Hz increase. The enhanced coordination of inverters is also highlighted by the P and Q trajectories (P_{pr} and Q_{pr}), as shown in Fig. 10(c) and (d), demonstrating smooth and efficient load sharing post-load step. This indicates the proposed control mechanism allows inverters to autonomously coordinate and share loads, a crucial aspect for harmonized control among parallel inverter-based energy resources in hybrid PV plants.

V. Conclusion

This paper has introduced a novel and unified coordinating GFM control strategy for inverter-based energy resources in hybrid PV plants, grounded in the concept of a new time-varying impedance concept. Verified through extensive MATLAB/Simulink simulations, this innovative control method has exhibited substantial improvements in both stability and dynamic performance compared to existing droop-based GFM control. The proposed method facilitates independent and coordinated control of f and V and enables effective power sharing among inverter-based energy resources and across multiple hybrid PV plants.

A notable aspect of this coordinating GFM controller is its reliance on a straightforward, robust P-f and Q-V droop mechanism, which operates effectively without the need for any communication infrastructure. This approach can reduce costs and mitigate the risk of cyberattacks while maintaining high system performance.

Appendix

TABLE I
Parameters and System Settings

Parameter	Symbol	Value
Voltage setpoint	E_0	480 V
Nominal frequency	f_0	60 Hz
Active power setpoint	P_o	6 MW
Reactive power set point	Q_0	0 kVar
DC voltage of inverters	V_{dc}	850 V
Cut off frequency	w_f	100 rad/s

References

[1] U.S. House and Senate, 117th Congress, 1st Session, *H.R. 1512, CLEAN Future Act.*, Mar. 2021. [Online]. Available: https://www.congress.gov/bill/117th-congress/house-bill/1512/text

[2] V. Gevorgian et al., "Hybrid utility-scale PV-wind storage plants for dispatchability and reliability services," National Renewable Energy Laboratory, Golden, CO, USA. Rep. no. NREL/PR-5D00-71551, May 8, 2018. [Online]. Available: chrome-extension://efaidnbmnnnibpcajpcglclefindmkaj/https://www.nrel.gov/docs/fy18osti/71551.pdf

[3] F. Katiraei and J. R. Agüero, "Solar PV integration challenges," *IEEE Power Energy Mag.*, vol. 9, no. 3, pp. 62–71, May/Jun. 2011.

[4] R. A. Walling and K. Clark, "Grid support functions implemented in utility-scale PV systems," in *Proc. IEEE PES T&D Conf.*, 2010, pp. 1–5.

[5] V. Gevorgian and B. O'Neill, "Advanced grid-friendly controls demonstration project for utility-scale PV power plants," National Renewable Energy Laboratory, Laboratory, Golden, CO, USA. Rep. no. NREL/TP-5D00-65368, Jan. 2016. [Online]. Available: chrome-extension://efaidnbmnnnibpcajpcglclefindmkaj/https://www.nrel.gov/docs/fy16osti/65368.pdf

[6] NERC Inverter-Based Resource Performance Task Force (IRPTF), "Fast frequency response concepts and bulk power system reliability needs," White Paper, Mar. 2020. [Online]. Available: chrome-extension://efaidnbmnnnibpcajpcglclefindmkaj/https://www.nerc.com/comm/PC/InverterBased%20Resource%20Performance%20Task%20Force%20IRPT/Fast_Frequency_Response_Concepts_and_BPS_Reliability_Needs_White_Paper.pdf

[7] S. Yu, S. Rong, and L. He, "Performance of grid-forming control of grid-edge DERs in distribution grids," in *Proc. IEEE Power Energy Soc. Gen. Meeting*, 2022, pp. 1–5.

[8] K. V. Kkuni, M. Nuhic, and G. Yang, "Power system stability impact assessment for the current limits of grid supporting voltage-source converters," in *Proc. IEEE Power Energy Soc. Gen. Meeting*, 2021, pp. 1–5.

[9] S. Bennai, A. B.-B. Abdelghani, I. Slama-Belkhodja, and M. Khalfoun, "Sensitivity analysis to grid line impedance for grid characterization and stability assessment investigations," in *Proc. IEEE Int. Conf. Elect. Sci. Technol. Maghreb*, 2022, pp. 1–6.

[10] J. M. Guerrero, L. Hang, and J. Uceda, "Control of distributed uninterruptible power supply systems," *IEEE Trans. Ind. Electron.*, vol. 55, no. 8, pp. 2845–2859, Aug. 2008.

[11] M. Prodanovic and T. C. Green, "High-quality power generation through distributed control of a power park microgrid," *IEEE Trans. Ind. Electron.*, vol. 53, no. 5, pp. 1471–1482, Oct. 2006.

[12] J. A. P. Lopes, C. L. Moreira, and A. G. Madureira, "Defining control strategies for microgrids islanded operation," *IEEE Trans. Power Syst.*, vol. 21, no. 2, pp. 916–924, May 2006.

Authorized licensed use limited to: ULAKBIM UASL - Omer Halisdemir Universitesi. Downloaded on November 17,2024 at 06:12:21 UTC from IEEE Xplore. Restrictions apply.

[13] T.-F. Wu, Y.-K. Chen, and Y.-H. Huang, "3C strategy for inverters in parallel operation achieving an equal current distribution," *IEEE Trans. Ind. Electron.*, vol. 47, no. 2, pp. 273–281, Apr. 2000.
[14] R. H. Lasseter, "Smart distribution: Coupled microgrids," *Proc. IEEE*, vol. 99, no. 6, pp. 1074–1082, Jun. 2011.
[15] W. Du, Q. Jiang, M. J. Erickson, and R. H. Lasseter, "Voltage–source control of PV inverter in a CERTS microgrid," *IEEE Trans. Power Del.*, vol. 29, no. 4, pp. 1726–1734, Aug. 2014.
[16] Q.-C. Zhong and G. Weiss, "Synchronverters: Inverters that mimic synchronous generators," *IEEE Trans. Ind. Electron.*, vol. 58, no. 4, pp. 1259–1267, Apr. 2011.
[17] J. Liu, Y. Miura, and T. Ise, "Comparison of dynamic characteristics between virtual synchronous generator and droop control in inverter–based distributed generators," *IEEE Trans. Power Electron.*, vol. 31, no. 5, pp. 3600–3611, May 2016.
[18] M. Sinha, F. Dörfler, B. B. Johnson, and S. V. Dhople, "Virtual oscillator control subsumes droop control," in *Proc. Amer. Control Conf.*, 2015, pp. 2353–2358.
[19] P. Kundur, *Power System Stability and Control*, 1st ed. New York, NY, USA: McGraw-Hill, 1994.
[20] H. Han, X. Hou, J. Yang, J. Wu, M. Su, and J. M. Guerrero, "Review of power sharing control strategies for islanding operation of AC microgrids," *IEEE Trans. Smart Grid*, vol. 7, no. 1, pp. 200–215, Jan. 2016.
[21] Y. Liao, X. Wang, and F. Blaabjerg, "Passivity-based analysis and design of linear voltage controllers for voltage-source converters," *IEEE Open J. Ind. Electron. Soc.*, vol. 1, pp. 114–126, 2020.
[22] H. Deng, J. Fang, Y. Qi, Y. Tang, and V. Debusschere, "A generic voltage control for grid-forming converters with improved power loop dynamics," *IEEE Trans. Ind. Electron.*, vol. 70, no. 4, pp. 3933–3943, Apr. 2023.
[23] Z. Peng et al., "Droop control strategy incorporating coupling compensation and virtual impedance for microgrid application," *IEEE Trans. Energy Convers.*, vol. 34, no. 1, pp. 277–291, Mar. 2019.
[24] Y. Li and Y. W. Li, "Power management of inverter interfaced autonomous microgrid based on virtual frequency-voltage frame," *IEEE Trans. Smart Grid*, vol. 2, no. 1, pp. 30–40, Mar. 2011.
[25] L. He and C.-C. Liu, "Parameter identification with PMUs for instability detection in power systems with HVDC integrated offshore wind energy," *IEEE Trans. Power Syst.*, vol. 29, no. 2, pp. 775–784, Mar. 2014.
[26] *IEEE 14 Bus System*, Aug. 19, 1993. [Online]. Available: http://labs.ece.uw.edu/pstca/pf14/pg_tca14bus.htm
[27] SERC, "PRC-006-SERC-02: Standard for energy reliability and control (UFLS) performance," *SERC Reliability Corporation*, Charlotte, NC, USA, Feb. 2021.

Shiwen Yu (Graduate Student Member, IEEE) received the B.S. degree in electrical engineering and the M.S. degree in electric engineering from the Wuhan University of Technology, Wuhan, China, in 2017 and 2020, respectively. He is currently working toward the Ph.D. degree in electrical engineering with the University of Illinois Chicago, Chicago, IL, USA. His research interests include grid-forming control, power systems stability, and machine learning.

Lina He (Senior Member, IEEE) received the B.S. and M.S. degrees from the Huazhong University of Science and Technology, Wuhan, China, in 2007 and 2009, respectively, and the Ph.D. degree in electrical engineering from University College Dublin, Dublin, Ireland, in 2014. She is currently an Assistant Professor with the Department of electrical and Computer Engineering, University of Illinois Chicago, Chicago, IL, USA. She was a Project Manager and Senior Consultant with Siemens headquarters in Germany and Siemens U.S., from 2014 to 2017. Her research interests include modeling, control, and protection of power electronics based power systems, renewable energy integration, grid-forming control, HVDC control and operation, and wide-area protection and cybersecurity.

Authorized licensed use limited to: ULAKBIM UASL - Omer Halisdemir Universitesi. Downloaded on November 17,2024 at 06:12:21 UTC from IEEE Xplore. Restrictions apply.